Point Cloud Classification and Accuracy Analysis Based on Feature Fusion

Xiaochen WANG[1], Hongchao MA[1*], Liang ZHANG[2], Zhan CAI[3], Haichi MA[1]

1. *School of Remote Sensing and Information Engineering, Wuhan University, Wuhan* 430079, *China*; 2. *Faculty of Resources and Environmental Science, Hubei University, Wuhan* 430062, *China*; 3. *School of Resources Environment Science and Technology, Hubei University of Science and Technology, Xianning* 437000, *China*

Abstract: A method for land-cover classification was proposed based on the fusion of features generated from waveform data and point cloud respectively. It aims to partially overcome the ineffectiveness of many traditional classifiers caused by the fact that point cloud is lack of spectral information. The whole flowchart of the method are as follows: Firstly, Gaussian decomposition was applied to fit an echo full-waveform. The parameters associated with the Gaussian function were optimized by LM (Levenberg-Marquard) algorithm. Six and thirteen features were generated to describe the waveform characteristics and the local geometry of point cloud, respectively. Secondly, random forest was selected as the classifier to which the generated features input. Relief-F was used to rank the weights of all the features generated. Finally, features were input to the classifier one by one according to the weights calculated from feature ranking, where classification accuracies were evaluated. The experimental results show that the effectiveness of the fusion of features generated from waveform and point cloud for LiDAR data classification, with 95.4% overall accuracy, 0.90 Kappa coefficient, which outperform the results obtained by a single class of features, no matter whether they were generated from point cloud or waveform data.

Key words: airborne LiDAR; full-waveform data; feature fusion; land-cover classification

Citation:

1 Introduction

Fast and high-precision classification of land cover is the key to realize dynamic monitoring, evaluation and prediction of the environment[1]. However, it is a big challenge for the government and researchers that the complex combination of artificial and natural objects in urban[2]. Airborne LiDAR, one of the most popular active earth observation system that integrates high-precision inertial measurement unit (IMU), global positioning system (GPS), and laser scanning ranging system[3], which has been rapidly developed and widely used in the last two decades due to its advantage of fast speed, high resolution, and strong penetration ability.

Traditional LiDAR can only provide discrete three-dimensional point cloud data, which limits the accuracy of classification. Many scholars are committed to making up for the lack of physical information in point cloud by multi-source data fusion[4-8]. For example, Nornan et al.[9] adopted three different fusion methods to improve the spatial and spectral richness of the multi-spectral images and LiDAR data. Cao et al.[10] proposed an urban land cover classification method based on the multi-level fusion of hyperspectral imagery and LiDAR data by using the complementary of their advantages. Wang et al.[11] conducted a segmentation process to generate the roadside tree classification at object level based on the fusion of GF-2 and mobile LiDAR data. Nguyen et

Received date：****-**-**; accepted date：****-**-**

Foundation support: National High Resolution Earth Observation Foundation (11-H37B02-9001-19/22); National Natural Science Foundation of China (41601504); National Key R&D Program of China (2018YFB0504500)

First author: Xiaochen WANG (1998—), male, master, majors in airborne LiDAR point cloud and waveform data processing.

Email: xchwang@whu.edu.cn

Corresponding author: Hongchao MA

E-mail: hchma@whu.edu.cn

al.[12] fused high resolution LiDAR point clouds and WorldView-3 imagery for building extraction on the city scale and even larger. However, these above simultaneous multisource data fusion classification methods have a great limitation which is restricted by the requirements of data completeness[13]. Hence, a fast, efficient, simple and convenient method is urgently needed to solve the problem of insufficient physical information in conventional airborne LiDAR data.

In 2004, the airborne LiDAR scanning system LMS-Q560 produced by Riegl of Austria entered the market, announcing the arrival of full-waveform era[21]. Fundamentally different from classical analogous pulse detection methods, the full-waveform ALS systems not only capture the range for multiple pulse reflections but also digitize and record the received signal of the reflected laser energy at a small sampling interval (1-2 nanoseconds)[20]. The shape of received waveform depends on the waveform of the emitted laser pulse, laser path, and the reflectance properties of target surface. Based on this, end users can analyze the waveform by various algorithms, such as average square difference function[22], Gaussian decomposition[23], and wiener filter decovolution[24]. After that, high density point clouds and waveform features can be adopted to improve the effect of LiDAR application[14-19]. Jutzi et al.[24] used full-waveform data for distance detection which achieved to distinguish the stepped surface which is less than one-tenth of the pulse length in footprint. Furthermore, Wu et al.[25] discussed the application potential of full-waveform data in vegetation areas by two designed indicators. Koma et al.[26] classified the tree species in urban areas which result is satisfied, but its accuracy was still affected by vehicles, fences, and other interferences.

A novel method is proposed by comprehensively utilize the point cloud features and waveform features to classify the land cover in this paper. The key contributions of this work are summarized as follows: 1) the spatial geometric information and physical information of ground objects are simultaneously employed which achieved a high accuracy land cover classification. 2) the weight of all features are calculated and sorted, and then the influence of each feature on different objects are analyzed.

2 Methodology

The main technology process of land cover classification method based on full-waveform data are composed of the following steps: pre-processing, waveform decomposition, feature extraction, and classification. And the whole workflow of the method proposed in this paper is shown in Fig.1.

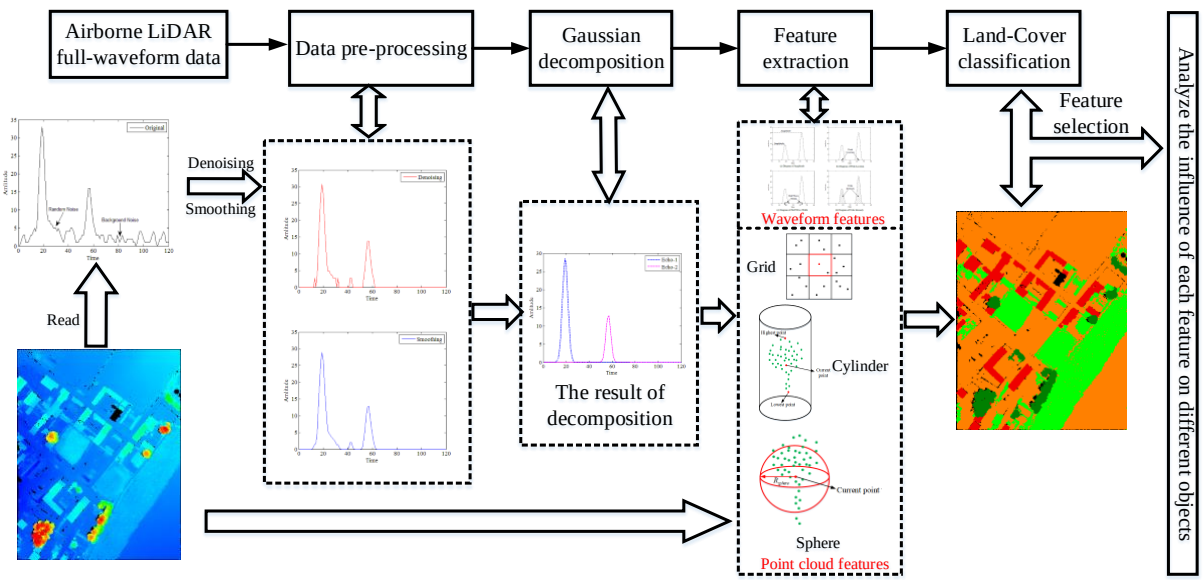

Fig.1 Experimental framework

2.1 Pre-processing

Full-waveform data of ALS is affected by the environment and sensor itself to generate some noise in the acquisition process. As shown in Fig.2 (a), these noises are small jitters in the original waveform which can be incorrectly judged as peaks. Hence, the number of detected peaks is far greater than the true value and interferes with the subsequent waveform processing steps.

These 'jitters' in the originally received waveform (Fig.2 (a)) can be divided into background noise and random noise based on the factors causing them. Aiming at background noise, the average of five percent of the front and tail is set to the standard noise value, and then the sample data whose value is smaller than stand noise threshold is corrected to zero which is shown in Fig.2 (b). For random noise, we adopted a Gaussian template in which window size is five to smooth the waveform data, and the result is shown in Fig.2 (c). The waveform data after all noise removal is shown in the blue curve in Fig. 2(c) which removes the effect of noise and remains main waveform information (amplitude, peak position, etc).

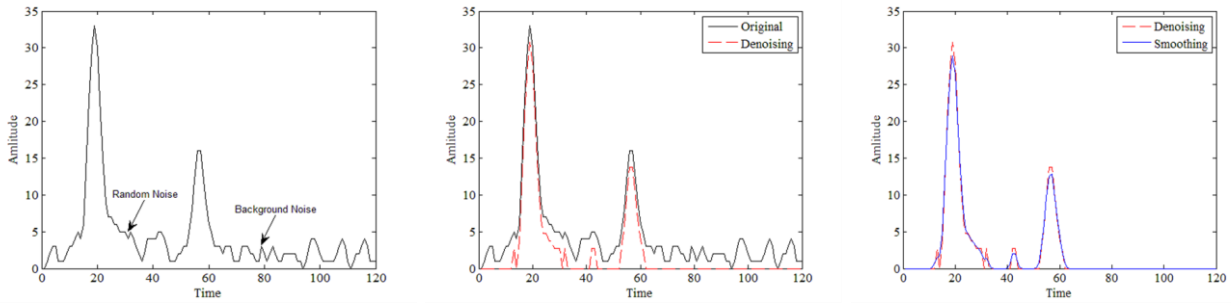

(a) Original waveform (b) Threshold denoising (c) Gaussian smoothing

Fig.2 Waveform data pre-processing, (a) the shape of original waveform; (b) the result after threshold denoising; (c) the result after Gaussian smoothing.

2.2 Gaussian decomposition

Gaussian decomposition is to model the airborne waveform data as a series of Gaussian distribution functions. Thus, full-waveform data can be described by:

$$y = f(x) = \frac{\sum_{i=1}^{n} A_i e^{-(x-\mu_i)}}{2\omega_i^2} + N_i \qquad (1)$$

Where, n is the number of echoes, A_i is the amplitude of echo, μ_i is the location of peaks, ω_i is half-wave width and N_i represents the influence of noise which has been removed in section 2.1.

Each gaussian echoes in the waveform are described by the parameters A_i, μ_i, and ω_i in equation (1). Whereby the Gaussian decomposition is to solve $3N$ unknown parameters of N echoes, which the optimal value is obtained by non-linear least square methods, such as Levenberg-Marquardt (LM). The implementation of Gaussian decomposition in this paper can be summarized as following three main steps:

***Step1*:** the number of echoes is defined as the number of peaks, that is, zero-crossing points, which can be detected by the first derivative.

***Step2*:** the initial value of waveform parameters μ_i^0 and ω_i^0 are determined by second derivative, which is respectively described in equations (2) and (3). Besides, the initial value of amplitude A_i^0 is estimated by the corresponding energy value of μ_i^0.

$$\mu_i^0 = (l_{2i-1} + l_{2i})/2 \qquad (2)$$

$$\omega_i^0 = |l_{2i-1} - l_{2i}|/2 \qquad (3)$$

Where, μ_i^0 is the initial value of peak location, ω_i^0 is the initial value of half-wave width, l_{2i-1} and l_{2i} are the position of echo inflection points.

***Step3*:** Levenberg-Marquardt (LM) method is employed to efficiently optimize the initial value of waveform parameters.

After the above steps, the waveform data are decomposed into a number of Gaussian echoes, which as shown in Fig.3.

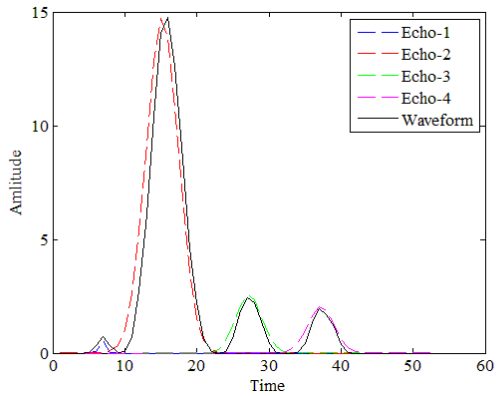

Fig.3 Results of full-waveform data Gaussian decomposition, the black solid line is the waveform data after preprocessed; the dotted line (blue, red, green, and purple) are respectively four Gaussian echo components after waveform decomposition.

Although the Gaussian echoes have been properly distinguished from each other in Fig.3, it also should be mentioned that not all waveforms are decomposed easily in the real situation. The number, location and shape of Gaussian echo are closely related to the ground objects encountered with laser scanning pulse. For example, due to the low vegetation is too closed to the bare ground surface, the adjacent laser scanning pulses will be superimposed on each other[27]. And the degree of superimposition depends largely on the time delay of Gaussian echoes, that is corresponding to the distance of different objects (time delay multiplies the speed of light).

2.3 Feature extraction

The original airborne LiDAR data generally have the information of 3D coordinate, intensity, and color. These limited pieces of information are satisfied for simple classification in flat terrain areas, but it's insufficient for complex terrain or multi ground objects classification. Hence, it is necessary to extract features that can better describe the differences between ground objects.

2.3.1Waveform features

Based on the parameters obtained from Gaussian decomposition, we generated waveform features such as amplitude, peak position, half-wave width, number of echoes, echo intensity and backscattering coefficient, which are used to describe the physical information of ground objects. Further, the meaning of these 6 features and calculation are described as follows:

(1) Amplitude: One of the waveform parameters optimized by LM algorithm, which changes with the radiation and geometric performance of different ground objects. And the research shows that grass and bare soil have a higher amplitude value, while the amplitude value of buildings depends on their roof materials[28].

(2) Peak position: The waveform parameter μ_i optimized by LM algorithm is the location of peak. It represents the time interval between the transmitting pulse response to target and the initial recording of echo pulse, i.e., the distance between the sensor and the laser point.

(3) Half-wave width: The waveform parameter ω_i optimized by LM algorithm is half-wave width, which is closely related to the category of ground objects.

(4) Number of echoes: The number of Gaussian echo components. In most cases, the bare soil and roof only have one echo, while the rough surface such as vegetation has multiple echo components.

(5) Echo intensity: It is defined as the value of energy reflected from the target to sensor, and can be calculated as equation (4):

$$intensity = \sqrt{2\pi} A_i \omega_i \tag{4}$$

Where, A_i is the amplitude, ω_i is the half-wave width.

(6) Backscattering coefficient: The backscattering coefficient γ is a standard standardized physical property, which represents the backscattering cross section per unit laser beam coverage area. And can be calculated as equation (5):

$$\gamma = \frac{\sigma}{A_{laser}} \tag{5}$$

Where, σ is backscattering cross-section, A_{laser} is

the area covered by the laser beam and can be calculated as equation (6):

$$A_{laser} = \frac{\pi R^2 \beta^2}{4} \quad (6)$$

Where, R is the distance from the sensor to the ground, β is the divergence angle of the emitting laser beam.

The backscattering cross-section σ is defined as the effective collision area between laser pulse and ground, which can be calculated as equation (7):

$$\sigma = C_{cal} R^4 \frac{A\omega}{\alpha^2} \Gamma(\frac{1}{\alpha^2}) \quad (7)$$

Where, C_{cal} is the calibration constant and can be calculated as equation (8), Γ is a gamma function that represents the effect of sensor on the echo.

$$C_{cal} = \frac{\pi \rho_{asphalt} \beta^2}{R^2 A_{asphalt} \omega_{asphalt}} \quad (8)$$

Where, $A_{asphalt}$, $\omega_{asphalt}$, $\rho_{asphalt}$ represent the amplitude, half-wave width and reflection coefficient of asphalt respectively since the asphalt is considered as a Lambert in practical application.

2.3.2Point cloud features

Based on the spatial distribution of laser point, we extracted step-off count, elevation, profile and density correlation features which can describe the geometric information of point cloud.

(1) Step-off count[30]: It is a feature based on grid neighborhood. The main idea of calculating step-off count is as follows two steps: 1) Find eight adjacent directions in the grid where the current point is located. 2) Calculating the elevation difference of the neighbor grid cells. 3) Statistic the number of directions in which elevation difference is greater than the preset threshold.

(2) Elevation features: The elevation features are extracted based on a cylinder neighborhood in this paper. The neighborhood is a straight cylinder formed by the current points as center, the radius is $R_{cylinder}$, and regardless of the height limit. Hence, the two-dimensional Euclidean distance between the current point and the remaining points is only needed to determine a cylinder neighborhood, as shown in equation (9).

$$\sqrt{(x_i - x_j)^2 + (y_i - y_j)^2} \leq R_{cylinder} \quad (9)$$

Where, $R_{cylinder}$ is the radius of cylinder, (x_i, y_i) is the plane coordinates of current point, (x_j, y_j) is the plane coordinates of searching point.

(3) Profile features: Similar to the elevation features, the profile features are also extracted based on the cylinder neighborhood. In this paper, the profile of cylinder is divided into several grids according to a certain height (0.5 m).

(4) Density features: The density features are extracted based on a sphere neighborhood in this paper. It is a collection of all laser points in the sphere formed by the current point as center and R_{sphere} as the radius. Similar to equation (9), it can be calculated by:

$$\sqrt{(x_i - x_j)^2 + (y_i - y_j)^2 + (z_i - z_j)^2} \leq R_{sphere} \quad (10)$$

Where, R_{sphere} is the radius of sphere, (x_i, y_i, z_i) is the coordinates of current point, (x_j, y_j, z_j) is the coordinates of searching point.

Since the laser scanning point clouds data are voxelized, discrete and have different densities, the derived features are related to the scale of neighborhood. However, research by Weinmann et al.[29] has shown that choosing different size of grid, cylinder and sphere neighborhood has a certain impact on the classification accuracy, but it is not significant. In this paper, according to the existing literature[30-32], combined with the density and the ground objects distribution of experimental data, the side length of grid neighborhood is set to 5m, the radius of cylinder and sphere neighborhoods are set to 3m.

2.4 Classifier and feature selection

Airborne LIDAR point cloud processing generally involves a large amount of data, consequently, it is a challenge to analyze the data quickly and accurately. Random forest (RF) classifier is an ensemble learning method based on the decision tree[33]. It has advantages over other classifiers in terms of processing speed,

imbalance of sample, and generalization ability for the multi-classification of massive point cloud data.

Feature selection is an operation of selecting a subset from all features, which enables researchers to discover the additional value of waveform features for point cloud classification. Besides, it can remove the interference of redundant features which not only have not improved the classification effect but may also have a negative impact[34]. The algorithm of feature selection can be broadly categorized into three classes: filter, wrapper, and embedded methods[35]. Among them, the filter feature selection algorithm is independent of the classification process and can be easily extended to high-dimensional data sets[36]. Moreover, the evaluation result of filter feature selection method can be directly applied in the different classifiers. In the various filter feature selection methods, the Relief-F[37], based on the improvement of Relief[38], has become one of the most successful algorithms which have efficient performance and can be employed to the multi-classification.

Based on the above mentioned, the Relief-F algorithm is adopted to evaluate the weight of waveform and point cloud features. After that, all the features are gradually input into the Random forest classifier by forward selection strategy, and the impact of different features on the classification of ground objects is analyzed according to the evaluation results. The key implementation steps of Relief-F algorithm are shown in Fig.4.

Relief-F algorithm

Input: Training sample **R** (the value of features to be evaluated and corresponding labels)
Output: The vector of the feature weight **W**

***Step1*:** Set the weight of all features to 0, **W** = 0;
***Step2*:** Repeat the following process *m* times
Step2.1: Randomly select a sample x_i
Step2.2: Find *k* nearest neighbor (*k* set to 10) sample **H** from the same label of the current point.
Step2.3: Find k nearest neighbor (k set to 10) sample **M** from the different label of the current point.
Step2.4: Calculate the weight of each feature.

$$W[A] = W[A] - \sum_{j=1}^{k} \frac{diff(A, r_i, h_j)}{(m.k)} + \sum_{c \neq class(r_i)} \frac{[\frac{p(c)}{1 - class(r_i)} \sum_{j=1}^{k} diff(A, r_i, h_j)]}{(m.k)}$$

Fig.4 Implementation of Relief-F algorithm

3 Experimental Results and Analysis

3.1 Experimental data

Based on the pre-processing, Gaussian decomposition, feature extraction, classification, and feature selection methods detailed in section 2, a real airborne waveform dataset is tested. The experimental data is from Beijing, China, covering approximately 40,530 square meters, with a point density of about 5 points/m^2. And the accurate label of laser points, such as ground, building, low vegetation, and high vegetation, is manually marked in commercial software LiDAR_Suite v4.6 provided by Wuhan Tianqing space information technology co., ltd. Furthermore, to solve the problem of different type of laser points are unevenly distributed, the training samples are manually selected, which is strived to satisfy the following three characteristics[39]:

1) It can represent the terrain distribution of the experimental data area.

2) Contains all labels of experimental data

3) Samples are evenly distributed in the experimental data area.

As shown in Fig.5, the whole experimental area is divided into 5 * 5 grids, and five of them are selected as training samples.

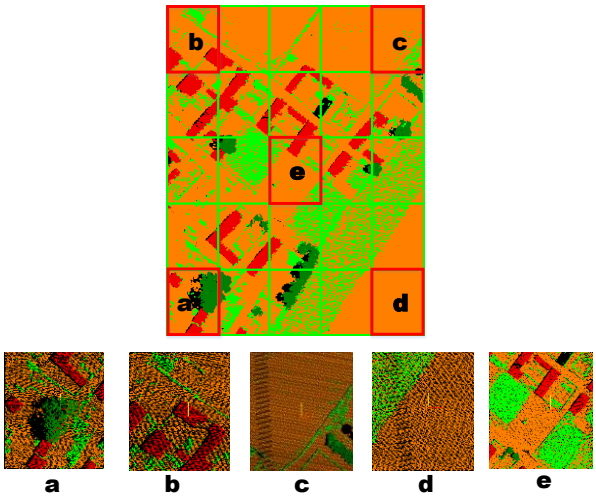

Fig.5 Manually classify experimental data and select training areas

3.2 Accuracy evaluation and comparison

At first, the feature fusion without selection is adopted to classify the experimental data, i.e., waveform features and point cloud features are directly combined without other operations. The classification result and ground truth of experimental area are shown in Fig.6.

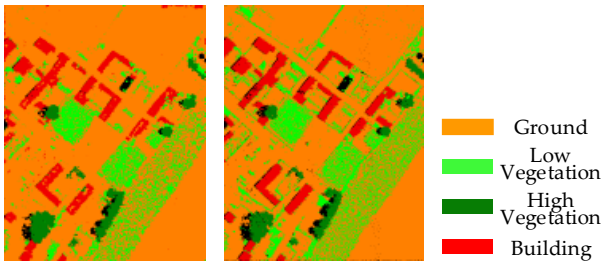

Fig.6 Classification effect of non-selective feature fusion, (a) has shown the data with semantic labels assigned by random forest classifier, (b) has shown the ground truth of experimental area. (Ground: brown, Low Vegetation: light-green, High Vegetation: dark-green, Building: red)

Based on the visual analysis, it can be concluded that the overall accuracy is satisfying, but there are still two obvious problems as follows: 1) part central area of the roof surface is confused with the bare ground. 2) some ground points are confused with vegetation and building in the upper area of experiment.

The above visual analysis of experimental result is sketchy and subjective. Thus, a confusion matrix is employed to further evaluate its accuracy, as shown in Table 1.

Table 1 Accuracy assessment of non-selective fusion classification results based on waveform features and point cloud features

		Predicted Label				
		Ground	Low-vegetation	High-vegetation	Building	Omission (%)
True Label	Ground	132844	1664	214	1745	2.65
	Low-vegetation	2951	29488	198	409	10.77
	High-vegetation	8	251	9932	33	2.86
	Building	1017	338	83	11770	10.89
	Commission(%)	2.91	7.10	4.75	15.67	
		Overall Accuracy: 95.4%		Kappa Coefficient: 0.90		

From the data analysis in Table 1, it can be seen that using the fusion of waveform features and point cloud features to classify the experimental data has a satisfactory effect, with an overall accuracy of 95.4% and Kappa coefficient of 0.90. The classification results of ground and high-vegetation is good, which have small commission and omission errors. However, the classification result of building and the classification of low-vegetation are comparatively poor, due to they are confused with ground points. For example, in the central roof surface, building points are wrongly divided into ground and the similar situation is found in the low vegetation points which are very close to bare ground surface.

The above experiment shows that directly combined waveform and point cloud features can achieve a good result. However, the high dimensional feature vector will bring enormous computational cost and a simple combination does not help us to understand the correlation between these features. Hence, the Relief-F algorithm introduced in section 2.4 is adopted to select those useful features and the

weight of each feature is evaluated based on the manual training samples in section 3.1. The ranking result is shown in Fig.7.

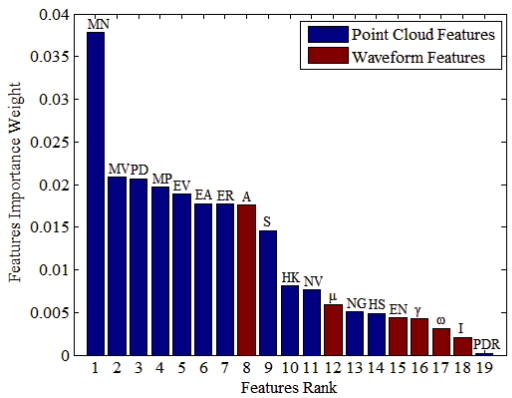

Fig.7 Feature ranking by Relief-F algorithm

It can be concluded from Fig. 7 that the amplitude A has a good performance in waveform features, and the maximum negative elevation difference MN, maximum positive elevation difference MP, maximum grid elevation variance MV, point cloud density PD, and elevation variation range ER have a high weight in the ranking.

Based on the result of feature ranking by Relief-F algorithm, we successively add features to analyze the impact of each kind of ground object. Besides, the omission and commission errors of ground, low-vegetation, high-vegetation, and building in the experimental data were calculated. Their changing trends were shown in Fig. 8.

It can be concluded from Fig.8 (a) that the commission error of ground is significantly reduced after the first five features (maximum negative elevation difference MN, maximum grid elevation variance MV, point cloud density PD, maximum positive elevation difference MP, elevation variance EV) and the eighth feature (amplitude A) were added. However, after adding the 9th-10th features (step-off count S, kurtosis of height difference HK), the omission error of ground increases greatly and the commission error also has fluctuated. It can be concluded from Fig.8 (b) that the omission and commission errors of low-vegetation decreased sharply after the first five features were added. Moreover, the addition of subsequent features makes the omission error increased slightly, but the commission error decreased gradually. It can be concluded from Fig.8 (c) that the omission and commission errors of high-vegetation decreased gradually when the first eight features are added. After that, the omission error tends to be stable but the commission error increased by a large margin when the 9th-10th and 14th (skewness of height difference HS) features were added. It can be concluded from Fig.8 (d) that the omission error of building is greatly affected by the first four features and then tends to be stable which similar to high-vegetation. The commission error of building has a down overall tend, but also there are big fluctuations. For instance, it was increased when the 3th, 6th, and 15th features (maximum grid elevation variance MV, average of elevation difference EA, echo number EN) were added. But it was decreased obviously when the 5th, 9th, 13th, and 17th features (elevation variance EV, step-off count S, Number of non-empty grids NG, Half wave width ω) were added.

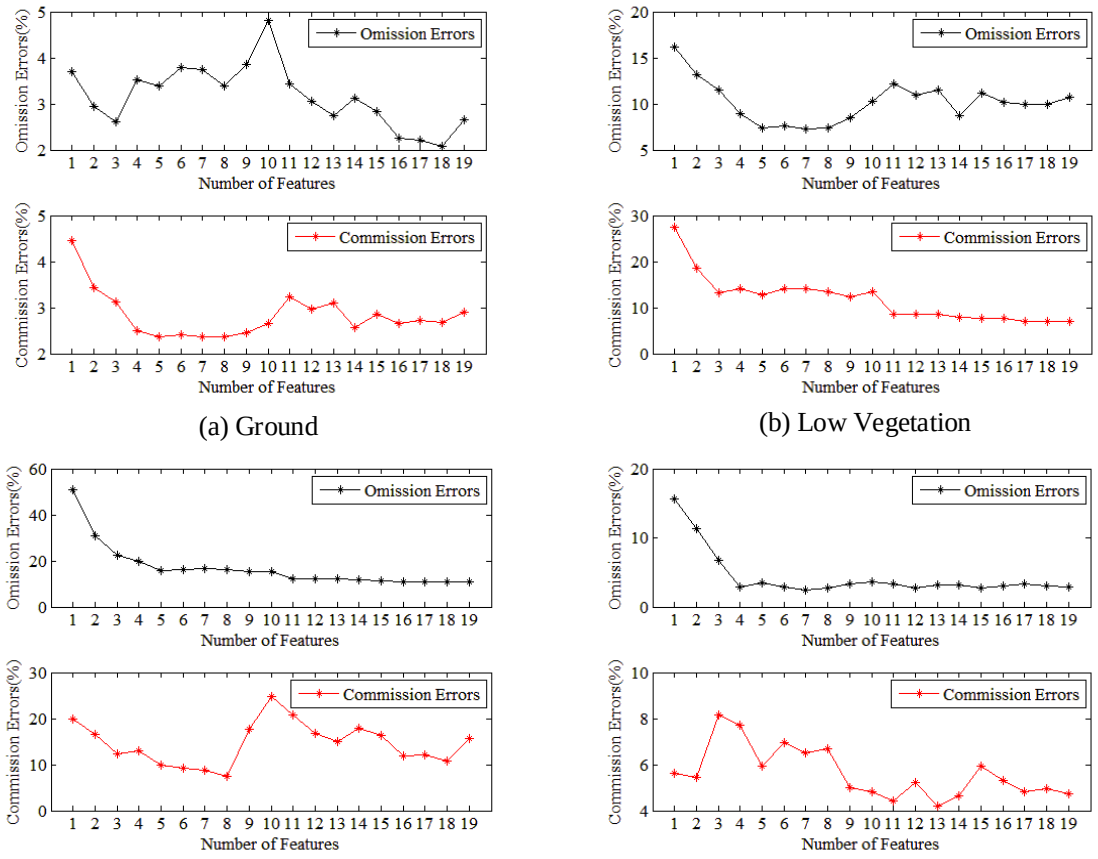

(a) Ground (b) Low Vegetation

(c) High Vegetation (d) Building

Fig.8 Error trend of the single category, black line and red line represent omission and commission errors respectively, (a) represents Ground, (b) represents Low-vegetation, (c) represents High-vegetation, (d) represents Building.

After that, four experiments with different feature combinations are designed to quantitatively evaluate and compare the impact of waveform features on the classification of ground objects. The statistical result is shown in Table 2, and it can be concluded that the fusion of two types of features can greatly improve the accuracy of only using waveform or point cloud features. Besides, the first 14 features according to the Relief-F algorithm ranking results are selected to classify experimental data, which achieves an overall accuracy of 95.31%. Finally, the classification effect of our method is compared with TerraScan in commercial software TerraSolid, and the result shows that our method is significantly superior to TerraScan.

Table 2 Statistics of experimental results

	Point cloud		Waveform		Point cloud& waveform		Relief-F (first 14 features)		TerraScan	
	I	II	I	II	I	II	I	II	I	II
ground	4.03	3.22	7.45	13.23	2.65	2.91	3.12	2.56	26.5	1.63
low-vegetation	11.8	8.56	33.5	30.86	10.7	7.10	8.73	7.81	5.59	55.32
high-vegetation	2.59	4.56	63.6	32.65	2.86	4.75	3.23	4.64	8.21	16.45
building	11.7	23.75	48.1	31.92	10.9	15.67	11.9	17.88	26.5	1.74
Overall Accuracy	94.20		82.33		95.40		95.31		78.07	

4 Conclusion

For the experimental area where contains complex distribution, six waveform features are introduced by Gaussian decomposition and combined with thirteen conventional point cloud features to classify different type ground objects. The three research conclusions are drawn as follows:

(1) The satisfactory classification effect can be achieved by using the fusion of point cloud features and waveform features, overall accuracy 95.4% with Kappa coefficient 0.90. However, simultaneously, there are problems of confusion between building, low-vegetation and ground.

(2) Based on the ranking result of Relief-F algorithm, it can be concluded that amplitude A has a good performance in waveform features. Moreover, the maximum negative elevation difference MN, maximum positive elevation difference MP, maximum grid elevation variance MV, point cloud density PD, and elevation variation range ER are performing well in the point cloud features, which have a high weight in the classification process.

(3) Waveform and point cloud features are gradually added to classify the ground objects, and then evaluate the result of each experiment. It can be concluded that the classification result of ground, low-vegetation, high-vegetation, and building are all improved by adding the first five and eighth features (maximum negative elevation difference MN, maximum grid elevation variance MV, point cloud density PD, maximum positive elevation difference MP, elevation variance EV, and amplitude A). However, there are also negative effects of some features on the classification, such as the errors of ground and high-vegetation have been increased when the step-off count S and kurtosis of height difference HK are added.

To sum up the above mentioned, a novel land-cover classification method was proposed based on the airborne LiDAR waveform data, and the influence of different features has been analyzed, which is of great significance to the processing and application of waveform data.

References

[1] ELIZAROV V V, GRISHKANICH A S, KASCHEEV S V, et al. Lidar scanning module for remote environmental monitoring[C]// International Conference Laser Optics (LO). Russia: IEEE, 2016.

[2] DONG W, LAN J, LIANG S, et al. Selection of LiDAR geometric features with adaptive neighborhood size for urban land cover classification[J]. International Journal of Applied Earth Observation & Geoinformation, 2017, 60:99-110.

[3] SHAN J, TOTH C K. Topographic Laser Ranging and Scanning: Principles and Processing[M]. Boca Raton: CRC Press, 2009:3-7.

[4] LUO S, WANG C, XI X, et al. Fusion of airborne discrete-return LiDAR and hyperspectral data for land cover classification[J]. Remote Sensing, 2016, 8(1), 3.

[5] SANKEY T, DONAGER J, MCVAY J, et al. UAV lidar and hyperspectral fusion for forest monitoring in the southwestern USA[J]. Remote Sensing of Environment, 2017, 195:30-43.

[6] Awad M M. Toward Robust Segmentation Results Based on Fusion Methods for Very High Resolution Optical Image and LiDAR Data[J]. IEEE Journal of Selected Topics in Applied Earth Observations & Remote Sensing, 2017, 10(5):2067-2076.

[7] POLIYAPRAM V, WANG W, NAKAMURA R. A Point-Wise LiDAR and Image Multimodal Fusion Network (PMNet) for Aerial Point Cloud 3D Semantic Segmentation[J]. Remote Sensing, 2019, 11(24):2961.

[8] WANG X, LI P. Extraction of urban building damage using spectral, height and corner information from VHR satellite images and airborne LiDAR data[J]. ISPRS Journal of Photogrammetry and Remote Sensing, 2020, 159:322-336.

[9] NORMAN M, SHAFRI H. Z. M, MANSOR S, et al. Fusion of multispectral imagery and LiDAR data for roofing materials and roofing surface conditions assessment[J]. International Journal of Remote Sensing, 2020, 41(18):1-22.

[10] CAO Q, MA A, ZHONG Y, et al. Urban classification by multi-feature fusion of hyperspectral image and LiDAR data[J]. Journal of Remote Sensing, 2019, 23(5):892-903.

[11] WANG M, LIU R, LU X, et al. The use of mobile lidar data and Gaofen-2 image to classify roadside trees[J]. Measurement Science and Technology, 2020, 31(12):125005.

[12] NGUYEN T. H, DANIEL, S, GUERIOT, D, et al. Super-Resolution-Based Snake Model-An Unsupervised Method for Large-Scale Building Extraction Using Airborne LiDAR Data and Optical Image[J]. Remote Sensing, 2020, 12(11):1702.

[13] OZKAN S, AKAR G B. Hyperspectral Data to Relative Lidar Depth: An Inverse Problem for Remote Sensing[C]// IEEE/CVF Conference on Computer Vision and Pattern Recognition Workshops (CVPRW). Long Beach, America: IEEE, 2019.

[14] BRUGGISSER M, RONCAT A, SCHAEPMAN M, et al. Retrieval of higher order statistical moments from full-waveform LiDAR data for tree species classification[J]. Remote Sensing of Environment, 2017, 196:28-41.

[15] ZORZI S, MASET E, FUSIELLO A, et al. Full-Waveform Airborne LiDAR Data Classification Using Convolutional Neural Networks[J]. IEEE Transactions on Geoscience and Remote Sensing, 2019, 57(10):8255-8261.

[16] MARSELIS S, ABERNETHY K A, ALONSO A, et al. Evaluating the potential of full‐waveform lidar for mapping pan-tropical tree species richness[J]. Global Ecology and Biogeography, 2020, 29(10).

[17] YANG X, WANG C, XI X, et al. Extraction of Multiple Building Heights Using ICESat/GLAS Full-Waveform Data Assisted by Optical Imagery[J]. IEEE Geoscience and Remote Sensing Letters, 2019, PP(99):1-5.

[18] LAI X, YUAN Y, LI Y, et al. Full-Waveform LiDAR Point Clouds Classification Based on Wavelet Support Vector Machine and Ensemble Learning[J]. Sensors, 2019, 19(14):3191.

[19] SHINOHARA T, XIU H, MATSUOKA M. FWNet: Semantic Segmentation for Full-Waveform LiDAR Data Using Deep Learning[J]. Sensors, 2020, 20(12):3568.

[20] MALLET C, SOERGEL U, BRETAR F. Analysis of Full-Waveform Lidar Data for Classification of Urban Areas [J]. Photogrammetrie fernerkundung geoinformation, 2008, 5(5):37-49.

[21] MALLET C, BRETAR F. Full-waveform topographic lidar: State-of-the-art[J]. Isprs Journal of Photogrammetry and Remote Sensing, 2009, 64(1):1-16.

[22] RONCAT A, WAGNER W, MELZER T, et al. Echo Detection and Localization in Full-Waveform Airborne Laser Scanner Data using the Averaged Square Difference Function Estimator[J]. Photogrammetric Journal of Finland, 2008, 21:62-75.

[23] WAGNER W, ULLRICH A, DUCIC V, et al. Gaussian decomposition and calibration of a novel small-footprint full-waveform digitising airborne laser scanner[J]. Isprs Journal of Photogrammetry and Remote Sensing, 2006, 60(2):100-112.

[24] JUTZI B, STILLA U. Range determination with waveform recording laser systems using a Wiener Filter[J]. Isprs Journal of Photogrammetry and Remote Sensing, 2006, 61(2):95-107.

[25] WU J, VAN AARDT J A N, ASNER G P. A Comparison of Signal Deconvolution Algorithms Based on Small-Footprint LiDAR Waveform Simulation[J]. IEEE Transactions on Geoence and Remote Sensing, 2011, 49(6):2402-2414.

[26] KOMA Z, KOENIG K, HÖFLE B. Urban tree classification using full-waveform airborne laser scanning. Isprs Annals of Photogrammetry Remote Sensing and Spatial Informa, 2016, Sci. 3:185–192.

[27] MA H, ZHOU W, ZHANG L. DEM refinement by low vegetation removal based on the combination of full waveform data and progressive TIN densification[J]. ISPRS Journal of Photogrammetry and Remote Sensing, 2018, 146(DEC.):260-271.

[28] ALEXANDER C, TANSEY K, KADUK J, et al. Backscatter coefficient as an attribute for the classification of full-waveform airborne laser scanning data in urban areas[J]. ISPRS Journal of Photogrammetry and Remote Sensing, 2010, 65:423-432.

[29] WEINMANN M, JUTZI B, MALLET C. Semantic 3D scene interpretation: A framework combining optimal neighborhood size selection with relevant features[J]. ISPRS Annals of the Photogrammetry, Remote Sensing and Spatial Information Sciences. II-3. 181-188.

[30] GUO B, HUANG X, ZHANG F, et al. Classification of airborne laser scanning data using JointBoost[J]. ISPRS Journal of Photogrammetry and Remote Sensing, 2014, 92(1):124-136.

[31] DONG W, LAN J, LIANG S, et al. Selection of LiDAR geometric features with adaptive neighborhood size for urban land cover classification[J]. International Journal of Applied Earth Observation & Geoinformation, 2017, 60:99-110.

[32] GRESSIN A, CLÉMENT MALLET, JÉRÔME DEMANTKÉ, et al. Towards 3D lidar point cloud registration improvement using optimal neighborhood knowledge[J]. ISPRS Journal of Photogrammetry and Remote Sensing, 2013, 79:240-251.

[33] BREIMAN L. Random Forests [J]. Machine Learning, 2001, 45(1): 5-32.

[34] MALLET C, BRETAR F, ROUX M, et al. Relevance assessment of full-waveform lidar data for urban area classification[J]. Isprs Journal of Photogrammetry & Remote Sensing, 2011, 66(6S):S71-S84.

[35] CAI Z, MA H, ZHANG L. Feature selection for airborne LiDAR data filtering: a mutual information method with Parzon window optimization[J]. GIScience & Remote Sensing, 2019, 57(4):1-15.

[36] LI X. The study and application of feature selection algorithms based on Relief[D]. DaLian: Dalian University of Technology, 2013.

[37] KONONENKO I. Estimating attributes: Analysis and extensions of RELIEF[C]// European Conference on Machine Learning. Berlin: 1994.

[38] KIRA K, RENDELL L A. A Practical Approach to Feature Selection[C]// International Workshop on Machine Learning. Morgan Kaufmann Publishers Inc, 1992.

[39] MA H, CAI Z, ZHANG L. Comparison of the filtering models for airborne LiDAR data by three classifiers with exploration on model transfer[J]. Journal of Applied Remote Sensing, 2018, 12(1):1-18.